British Journal of Cancer www.nature.com/bjc

ARTICLE

Cellular and Molecular Biology

The CBS-H_2S axis promotes liver metastasis of colon cancer by upregulating VEGF through AP-1 activation

Shihao Guo[1,2], Jichang Li[1], Zhihao Huang[1], Taohua Yue[1], Jing Zhu[1], Xin Wang[1], Yucun Liu[1], Pengyuan Wang[1] and Shanwen Chen[1]✉

BACKGROUND: The main therapy for colon cancer with liver metastasis is chemotherapy based on 5-fluorouracil combined with targeted drugs. However, acquired drug resistance and severe adverse reactions limit patients' benefit from standard chemotherapy. Here, we investigate the involvement of endogenous hydrogen sulfide (H_2S) in liver metastasis of colon cancer and its potential value as a novel therapeutic target.

METHODS: We used the CRISPR/Cas9 system to knockdown CBS gene expression in colon cancer cell lines. PCR arrays and proteome arrays were applied to detect the transcription and protein expression levels, respectively, of angiogenesis-related genes after knockdown. The molecular mechanism was investigated by western blot analysis, RT–qPCR, immunofluorescence staining, ChIP assays and dual-luciferase reporter assays. A liver metastasis mouse model was adopted to investigate the effect of targeting CBS on tumour metastasis in vivo.

RESULTS: Knockdown of CBS decreased the metastasis and invasion of colon cancer cells and inhibited angiogenesis both in vivo and in vitro. Tissue microarray analysis showed a positive correlation between CBS and VEGF expression in colon cancer tissues. Further analysis at the molecular level validated a positive feedback loop between the CBS-H_2S axis and VEGF.

CONCLUSIONS: Endogenous H_2S promotes angiogenesis and metastasis in colon cancer, and targeting the positive feedback loop between the CBS-H_2S axis and VEGF can effectively intervene in liver metastasis of colon cancer.

British Journal of Cancer (2022) 126:1055–1066; https://doi.org/10.1038/s41416-021-01681-7

INTRODUCTION

Colorectal cancer (CRC) is the third most common cancer (10%) and the second most deadly cancer (9.4%) worldwide, with an increasing incidence rate [1]. Liver metastasis is the major contributor to mortality in patients with CRC. Up to 50–60% of patients with CRC will develop liver metastasis during the course of the disease. The 5-year survival rate of patients with liver metastasis after curative resection is as high as 42%, while the 5-year survival rate of patients without curative resection is only 9%. However, 85% of CRC patients with liver metastasis do not have access to curative resection [2]. Conversion therapy, that is, the conversion of initially unresectable liver metastases into resectable lesions through comprehensive treatment, has gained increased clinical attention. Currently, the overall success rate of conversion therapy is only 10–30%. The 5-year survival rate of patients with liver metastasis from colon cancer in whom conversion therapy failed is only 1–2%. Liver metastasis has become the most important factor leading to the poor prognosis of colon cancer [3]. Although the use of targeted drugs such as bevacizumab and cetuximab has significantly improved the success rate of conversion therapy to some extent, side effects and drug resistance limit their clinical benefit. Therefore, it is of great research value and clinical significance to explore new targets involved in liver metastasis of CRC and develop corresponding therapeutic drugs to improve the overall therapeutic effect.

After nitric oxide and carbon monoxide, hydrogen sulfide (H_2S) was the third gaseous signalling molecule to be confirmed in the human body [4]. Increased endogenous H_2S anabolism is one of the common metabolic characteristics of various tumour cells and plays an important role in multiple tumour biological behaviours, such as energy metabolism, antioxidant stress and chemotherapy resistance of tumour cells [5, 6]. In colon cancer, H_2S is mainly derived from the transsulfuration pathway, which is composed of cystathionine-β-synthase (CBS), cystathionine-γ-lyase (CSE) and 3′-mercaptopyruvate sulfur transferase (3-MPST). Accumulating studies have found that the levels of H_2S and its synthases in colon cancer tissues are significantly increased compared with those in adjacent normal tissues. Elevated endogenous H_2S can promote tumour proliferation and metastasis by improving cell energy metabolism and enhancing the tumour blood supply and antioxidative stress response [7–9]. The role of H_2S and its synthases in distant metastasis in a variety of tumours has received increased attention. Elevated endogenous H_2S plays a vital role in bone metastasis of prostate cancer, and depleting CSE can significantly inhibit bone metastasis of prostate cancer [10]. In

[1]Division of General Surgery, Peking University First Hospital, Peking University, 100034 Beijing, People's Republic of China. [2]Department of Colorectal Surgery, The First Affiliated Hospital of Zhengzhou University, Zhengzhou, China. ✉email: shanwen_chen@126.com

Received: 27 July 2021 Revised: 4 December 2021 Accepted: 16 December 2021
Published online: 24 December 2021

addition, H_2S promoted angiogenesis in non-small-cell lung cancer by activating VEGF [11]. Our previous studies showed that endogenous H_2S can facilitate acquired drug resistance to 5-FU by upregulating the expression levels of TYMS and EREG in colon cancer cells. Various H_2S-producing enzymes can be upregulated in drug-resistant cell lines [12], and inhibiting H_2S production can significantly reverse this resistance to 5-FU and oxaliplatin [13, 14].

The initiation, propagation and metastasis of tumours are closely related to the abundant neovascularisation in the tumour microenvironment [15]. H_2S is able to promote tumour-related angiogenesis, and the newly formed vessels fuel the proliferation and diffusion of tumour cells [16, 17]. In addition, tumour cells secrete paracrine H_2S into local tissues and dilate peripheral blood vessels [7, 11, 18]. Studies have shown that CRC cells can produce an increased amount of H_2S compared with normal cells through upregulation of CBS, leading to elevated diffusion of H_2S into the surrounding tumour microenvironment [7]. In addition, recent studies have shown that H_2S can promote the proliferation and migration of colon cancer cells and regulate the EMT/MET balance in colon cancer cells [19–22]. In this study, we investigated the role of endogenous H_2S in angiogenesis and metastasis in colon cancer and found that the positive feedback loop between the CBS-H_2S axis and VEGF plays an essential role in liver metastasis of colon cancer.

MATERIALS AND METHODS

Cell culture and the main reagents

We acquired the human colon cancer cell lines SW480 and DLD1 from the American Type Culture Collection (USA). The cell lines were authenticated by STR profiling, and their mycoplasma-free status was confirmed to be maintained through routine screening. SW480 cells were cultured in DMEM/high glucose (BI, ISR), and DLD1 cells were cultured in RPMI-1640 medium (BI, ISR); both media were supplemented with foetal bovine serum (10% v/v), penicillin (50 U/ml), streptomycin (50 U/ml), 1% nonessential amino acids and 25 mM HEPES. Cells were incubated in an environment of 37 °C and 5% CO_2.

GYY4137 was purchased from Sigma–Aldrich (MO, USA); sikokianin C was purchased from BioBioPha (Kunming, China); VEGF was purchased from Thermo Fisher (MA, USA); and bevacizumab was purchased from TargetMol (MA, USA).

CRISPR/Cas9-mediated knockdown of CBS in cells

The CRISPR/Cas9 system was used to achieve stable knockdown (KD) of CBS in SW480 and DLD1 cells. Briefly, the interference target sgRNA was designed based on the sequence of the CBS gene, as follows: CTGATGAGATCCTGCAGCAG. We phosphorylated and annealed the guide oligonucleotide and cloned it into the BsmBI site in the pHBLV-U6-gRNA-EF1-CAS9-PURO vector (Hanbio Biotechnology, China); we then verified the constructed vector by sequencing. Then, we transformed the transfer plasmid with the guide oligonucleotide sequence into *Escherichia coli* DH5α and used a Plasmid DNA Purification Kit (Macherey-Nagel, Germany) to isolate the plasmid from the bacterial cells. The transfer lenti-CAS-puro plasmid (Hanbio Biotechnology, China), packaging plasmid psPAX2 (Hanbio Biotechnology, China) and envelope plasmid pMD2.G (Hanbio Biotechnology Co., Ltd, China) were transfected into 293 T cells to produce lentiviruses. At 48 and 72 h after transfection, we collected the virus-containing supernatant and then used the supernatant to transduce SW480 or DLD1 cells. Fresh medium containing puromycin (10 mg/L) was utilised to replace the lentivirus-containing medium 16 h after infection. After 7 days of screening, we collected the puromycin-resistant cells. Finally, western blotting and sequencing of single clones were used to detect the cell transduction efficiency.

We cultured 10 single clones from each type of mass cell culture and verified the genotype of the single clones through Sanger sequencing. The sequencing results are shown in Figs. S1 and S2, which indicate that the percentage of knockout SW480 cell clones was 90% and the percentage of DLD1 cell knockout clones was 80%.

Real-time quantitative polymerase chain reaction (RT–qPCR)

We utilised the TRIzol one-step method (TRIzol reagent; Invitrogen, USA) to extract the total RNA of cells and a RevertAid First Strand cDNA Synthesis Kit (Thermo Fisher, USA) to reverse transcribe RNA into cDNA. PowerUp SYBR Green Master Mix (Thermo Fisher, USA) was used to conduct RT–qPCR. The primer sequences (5′-3′) were as follows: GAPDH—F, GCACCGTCAAGGCTGAGAAC and R, ATGGTGGTGAAGACGCCAGT; VEGF—F, GGGCAGAATCATCACGAAGTG and R, CACCAGGGTCTCGATTGGAT; CBS—F, TGGTGGACAAGTGGTTCAAGAGCAA and R, TGGTCATGTAGTTCCGCACTGAGTC; AP-1—F, ATGGAAACGACCTTCTATGACGATG and R, TTCAGGATCTTGGGGTTACTGTAGC; NF-κB—F, CACAAGGCAGCAAATAGACGA and R, GGGGCATTTTGTTGAGAGTTAG. RT–qPCR was repeated three times for each sample. GAPDH was used as the internal reference gene, and relative RNA expression levels were calculated by the comparative threshold cycle method ($2^{-\triangle\triangle CT}$).

Western blot analysis

A method described previously was used to extract total protein from cells [23]. The BCA method (Thermo Scientific, USA) was used to determine the protein concentration, and extracts containing the same amount of protein (20 μg) were electrophoresed on a 4–12% polyacrylamide gel. Separated proteins were transferred onto a PVDF membrane. Nonspecific binding on the membrane was blocked (5% bovine serum albumin in TBS-Tween 20 buffer) for 1 h at room temperature. Then, the membrane was incubated with 0.1% rabbit anti-CBS monoclonal antibody (Invitrogen #PA5-51544, USA), 0.1% rabbit anti-VEGF monoclonal antibody (Invitrogen #MA5-12184, USA), 0.1% rabbit anti-c-jun monoclonal antibody (Invitrogen #MA5-15172, USA), 0.1% rabbit anti-NF-κB antibody (CST #8242, USA) and 0.1% rabbit anti-GAPDH monoclonal antibody (CST #5174, USA) overnight at 4 °C. Then, we incubated the membrane with a horseradish peroxidase-conjugated secondary antibody (CST #7074, USA) for 1 h at room temperature and used an ECL detection reagent to visualise immunoreactions (Merck Millipore, USA).

H_2S determination

To detect the inhibition of cellular H_2S synthesis after CBS knockdown, a fluorescent probe kindly provided by Professor Long Yi was utilised. The probe was water-soluble, was cell membrane permeable, had low cytotoxicity, and had high selectivity and sensitivity for H_2S. It displayed an 87-fold fluorescence enhancement at 796 nm (with excitation at 730 nm) when reacted with H_2S in PBS (pH 7.4). The properties of the probe enable its use in monitoring endogenous H_2S in living cells [24]. Briefly, we used a glass-bottom plate (Corning, USA) to inoculate cells (~2×10^4 cells/well) and cultured the cells for 24 h. Then, the H_2S probe (10 μmol/L) was incubated with the cells for 30 min. Finally, the cells were washed twice with PBS, and the fluorescence of the cells in PBS buffer was visualised under a FluoView 1000 confocal microscope (Olympus, Japan).

Lead acetate test papers were also used to measure cellular H_2S synthesis. Briefly, we inoculated cells in a 96-well plate (1×10^3 cells/well), placed a strip of lead acetate test paper on top of the 96-well plate, and placed the plate in the incubator. After 24 h, the colour of the corresponding position on the test paper above each well was recorded to determine the amount of H_2S that had been released in the wells.

Transwell migration and invasion assays

Transwell chambers (8 μm pore size; Corning, USA) with or without Matrigel precoating were used for the migration and invasion assays, respectively. In brief, 3×10^4 cells were suspended in medium and seeded into the upper chambers. The lower chambers were filled with medium containing 10% FBS. After 24 h of incubation, cells that invaded through the pores were fixed with 4% paraformaldehyde for 20 min and stained with 1% crystal violet. The invaded cells were counted using a microscope (Olympus, Japan).

In brief, 3×10^4 cells were inoculated into the upper chambers of the Transwell plate. Medium containing 10% foetal bovine serum was added to the lower chambers of the Transwell plate. After 24 h, 4% paraformaldehyde was used to fix the cells for 20 min, the cells on the top surface of the membrane in the upper chamber were scraped off, and the cells that passed through the pores were stained with 1% crystal violet. Then, the cells were counted using a microscope (Olympus, Japan).

Tube formation assay

For the tube formation assay, a mixture containing 50 μL of BD Matrigel (Corning, USA) and 50 μL of the medium was used to coat the upper chambers of a Transwell plate (8 μm pore size; Corning, USA), and the plate was incubated at 37 °C for 30 min. Next, HUVECs (1×10^5 cells/well) were

seeded into the upper chambers, and SW480 or DLD1 cells were seeded into the lower chambers of the plate. After incubation for 6 h, the tubes were observed using a microscope (Olympus, Japan) and measured with ImageJ software to determine the tube formation ability. Each experiment was performed in triplicate.

Dorsal skinfold chamber model

The dorsal skinfold chamber model was established in mice as previously described with some modifications [25]. Briefly, male BALB/c-nu mice (20–22 g body weight) were anaesthetised (with inhaled isoflurane at 3% for maintenance) and placed on a heating pad. Two symmetrical titanium frames were implanted into a dorsal skinfold to sandwich the extended double layer of the skin. A layer of ~15 × 15 mm was excised. The surgical site was monitored for 48 h, and 1×10^6 WT or CBS-KD SW480 cells were then injected into the chamber window. Mice in the WT + GYY4137 group were injected intraperitoneally with 500 μg/10 g body weight GYY4137 6 days per week, and mice in the WT and CBS groups were injected intraperitoneally with 200 μL/10 g body weight PBS 6 days per week. After 2 weeks, the tumour cells were removed, and vascularisation of the dorsal skin inside the chamber windows was observed.

PCR array and proteome array analyses

An RT^2 Profiler PCR Array Human Angiogenesis Kit (Qiagen, Germany) was used for PCR array analysis, and a Proteome Profiler Array-Human Angiogenesis Array Kit (R&D, USA) was used for proteome array analysis. The analyses were carried out following the manufacturer's instructions.

Tissue microarray analysis and immunohistochemical scoring of stained tissues

Tissue microarrays were purchased from Alenabio (Xi'an, China), and they contained a total of 90 colon cancer tissues and paired adjacent normal tissues. Immunohistochemistry was performed as previously described [26]. Information on the patients and their tissues was offered by Alenabio (Xi'an, China). All patients provided written informed consent to use their biopsy samples. All of the methods used in this study were in accordance with the approved guidelines, and all of the experimental protocols were approved by the ethics committee of Peking University First Hospital.

The degree of immunostaining was assessed and scored by three independent observers in a double-blinded manner. The proportion of positive cells and the staining intensity were used as the evaluation criteria. In each sample, at least 1000 cells were analysed. According to the percentage of positive cells, scores were assigned as follows: less than 5%, 1 point; 6–35%, 2 points; 36–70%, 3 points; more than 70%, 4 points. In addition, according to the staining intensity, scores were assigned as follows: negative staining, 0 points; weak staining, 1 point; moderate staining, 2 points; and strong staining, 3 points. The final histochemical score (H-score) was obtained by multiplying the above two scores. The protein expression level in the tissues was evaluated according to the H-score: score: score ≥8, high; 4 ≤ score <8, moderate and 0 ≤ score <4, low.

ChIP assay

The ChIP assay was performed as described previously with a Pierce Magnetic ChIP Kit (Thermo Fisher, USA), rabbit anti-c-jun antibodies (Thermo Fisher #MA5-15172, USA), and rabbit anti-NF-κB antibodies (CST #8242, USA). Expression was quantified by PCR and gel electrophoresis using primers flanking the AP-1 sites in the promoter of the VEGF gene and primers flanking the NF-κB sites in the promoter of the CBS gene. The primer sequences (5′-3′) are listed as follows: AP-1, F-AAGATGTGGAGAGT TGGAGG and R-CCTGCGTGATGATTCAAACC; NF-κB, F-CACCGTCCGTGTC TTTCG and R-CGTTTCCCAAACATCGTGCTC.

Dual-luciferase reporter assay

Luciferase reporter vectors containing the VEGF and CBS promoters (VEGF-luc and CBS-luc) were purchased from Vigene Biosciences (Shandong, China); these vectors were constructed by ligating the VEGF and CBS promoter regions into the pGL3-Basic firefly luciferase reporter vector at the Xho I and Hind III restriction sites.

Cells were seeded in six-well plates and grown to 70–80% confluence; then, the cells in each well were transfected with VEGF-luc or CBS-luc. Next, the cells were treated according to their group for 48 h, and the dual-luciferase activity of the transfected cells was examined using the Promega Dual-Luciferase Reporter Assay system in a Promega GloMax 20/20 luminometer (both from Promega Corporation). The transcriptional activity of the VEGF or CBS gene promoter was expressed as the ratio of firefly luciferase activity to Renilla luciferase activity. The transcriptional activity of the VEGF and CBS gene promoters in the control group was set to 100%, and the relative transcriptional activity of the gene promoters in the other groups was calculated accordingly.

Immunofluorescence (IF)

AP-1 and NF-κB expression in cells was evaluated by immunofluorescence as described previously [27]. In brief, cells were washed with PBS, fixed with 100% methanol at −20 °C overnight, and then fixed with 100% acetone at −20 °C for 1 min. Next, the cells were washed with PBS and blocked with 1% BSA at room temperature for 2 h. Then, the cells were incubated with rabbit anti-c-jun antibodies (Thermo Fisher, USA) and rabbit anti-NF-κB antibodies (CST, USA) at 4 °C overnight. After washing with PBS, the cells were incubated with Alexa Fluor 488-conjugated goat anti-rabbit IgG (Molecular Probes, USA) or Alexa Fluor 555-conjugated goat anti-mouse IgG (Molecular Probes, USA) in 1% BSA at room temperature for 1 h. Then, the cells were washed with PBS and subsequently stained with propidium iodide. After washing with PBS, Prolong Gold anti-fade reagent (Molecular Probes, USA) was used to mount the coverslips; then, the slides were stored at 4 °C in the dark until analysis. Fluorescence was visualised under a Fluoview 1000 confocal microscope (Olympus, Japan).

In vivo metastasis assays

In vivo metastasis assays were performed as previously described [28]. Five-week-old male BALB/c nude mice were purchased from the Laboratory Animal Institute of Peking University Health Center (Beijing, China). WT or CBS-KD SW480 cells (1×10^6) in 200 ml of PBS were injected into the mouse liver via the spleen. Mice injected with WT cells were randomly divided into four groups: the control group, bevacizumab group, sikokianin C group, and bevacizumab + sikokianin C group. Mice injected with CBS-KD cells were randomly divided into two groups: the control group and the bevacizumab group. For random grouping, all mice were numbered and assigned to the different groups by a random number table. The process of drug administration was performed in a double-blinded manner. Drug administration began 14 days after the injection of tumour cells and continued for 3 weeks. Sikokianin C (0.2 mg/20 g body weight) was intraperitoneally injected 6 days a week. Bevacizumab (0.1 mg/20 g body weight) was intraperitoneally injected once a week. Five weeks after cell injection, mice in the six groups (5 mice/group) were sacrificed, and their livers were harvested. The metastases were counted, and HE staining was performed on serial sections of liver specimens to confirm metastasis. Immunohistochemical staining was also performed to detect the expression of VEGF and the number of microvessels in metastatic lesions. The experimental protocol complied with the Guide for Care and Use of Laboratory Animals and was authorised by the Institutional Animal Care and Use Committee of Peking University for the use of experimental animals (No. J201965).

Statistical analysis

We used two-tailed Student's *t*-test (unpaired) and one-way ANOVA to analyse differences in the mean values between two groups and among more than two groups, respectively (GraphPad Prism version 8.0 for Windows, GraphPad Software, USA). A *P*-value <0.05 was considered to indicate statistical significance (represented by * and #), and all results are expressed as the mean ± standard error of the mean (SEM) values. To ensure reproducibility, all experiments were repeated at least three times. Standard deviations are shown by error bars.

RESULTS

Inhibiting CBS decreased the migration and invasion of colon cancer cells

Our previous work validated the upregulation of the CBS-H_2S axis in colon cancer tissues. To further delineate the involvement of this axis in the metastasis of colon cancer, stable knockdown of CBS was achieved utilising CRISPR/Cas9 in both SW480 and DLD1 cell lines (Fig. 1a–f). The decreased intracellular H_2S level was validated by fluorescent probes after CBS knockdown in both cell lines (Fig. 1g). The inhibitory effect of sikokianin C, a newly identified CBS inhibitor, on the endogenous H_2S level was also

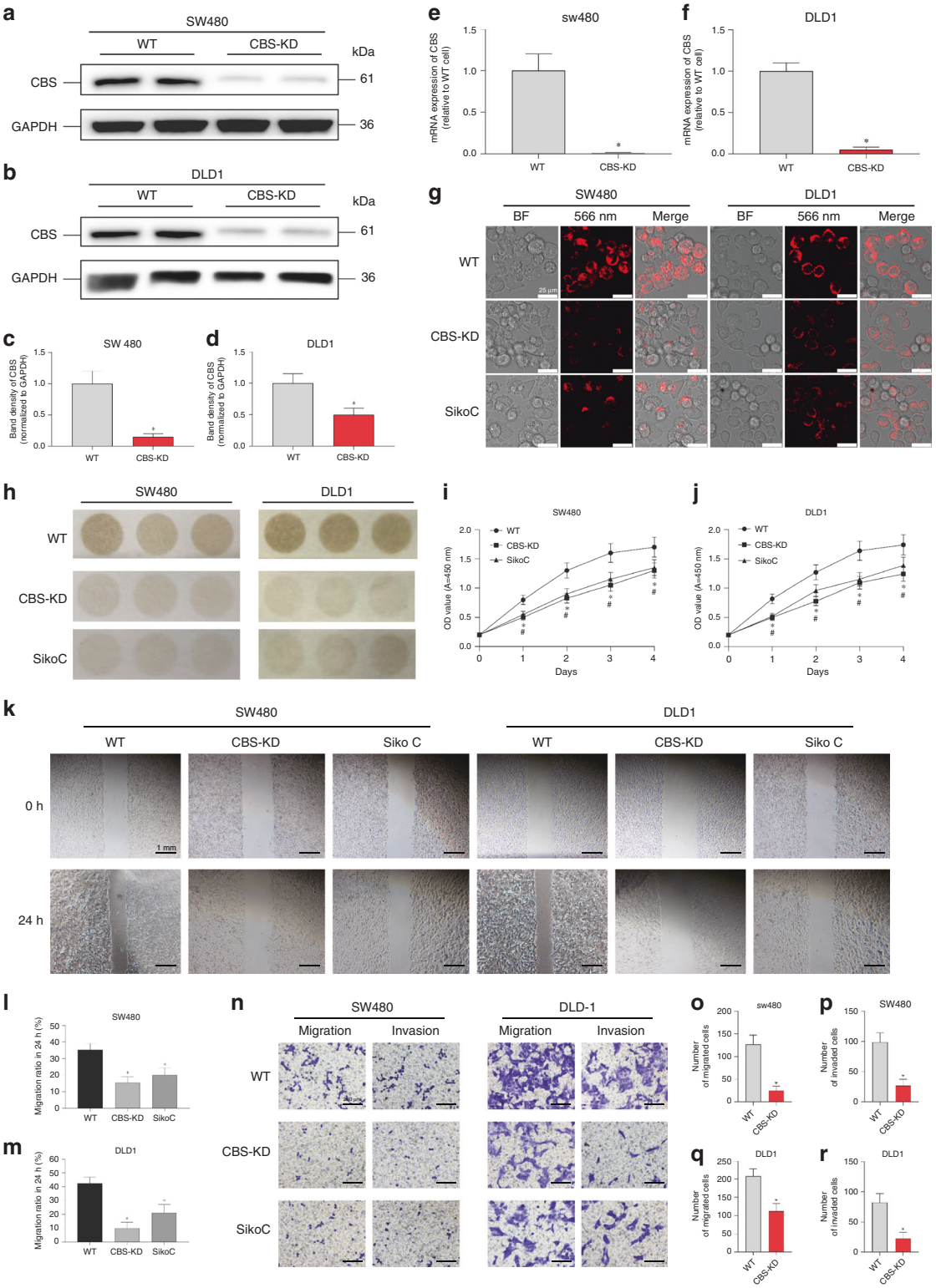

Fig. 1 Effects of CBS inhibition on H_2S production, invasion and metastasis in SW480 and DLD1 cells. a, b Representative western blot images of CBS in WT and CBS-KD SW480 cells and DLD1 cells. **c, d** Relative band density of CBS in western blot analysis. **e, f** mRNA expression levels in SW480 and DLD1 cells after CBS knockdown. **g** H_2S levels in different groups of cells, as measured by the H_2S probe. **h** H_2S levels in different groups of cells, as measured by lead acetate test paper. Cells in the sikokianin C group were treated with 1 μM sikokianin C for 48 h, as described below. **i, j** Proliferation of WT cells treated with or without sikokianin C and proliferation of CBS-KD cells. **k** Representative images of the scratch in different groups of cells. **l, m** Migration rate of SW480 and DLD1 cells at the edge of scratches in different groups in the scratch assay. **n** Representative images of migration and invasion through the membrane of Transwell chambers in different groups of cells. **o, p** Analysis of the number of SW480 cells that passed through the Transwell chamber membrane during the migration and invasion assays. **q, r** Analysis of the number of DLD1 cells that passed through the Transwell chamber membrane during the migration and invasion assays. ($n = 3$, biological replicates) $^{*}P < 0.05$ vs. the WT group. $^{\#}P < 0.05$ vs. the CBS-KD group.

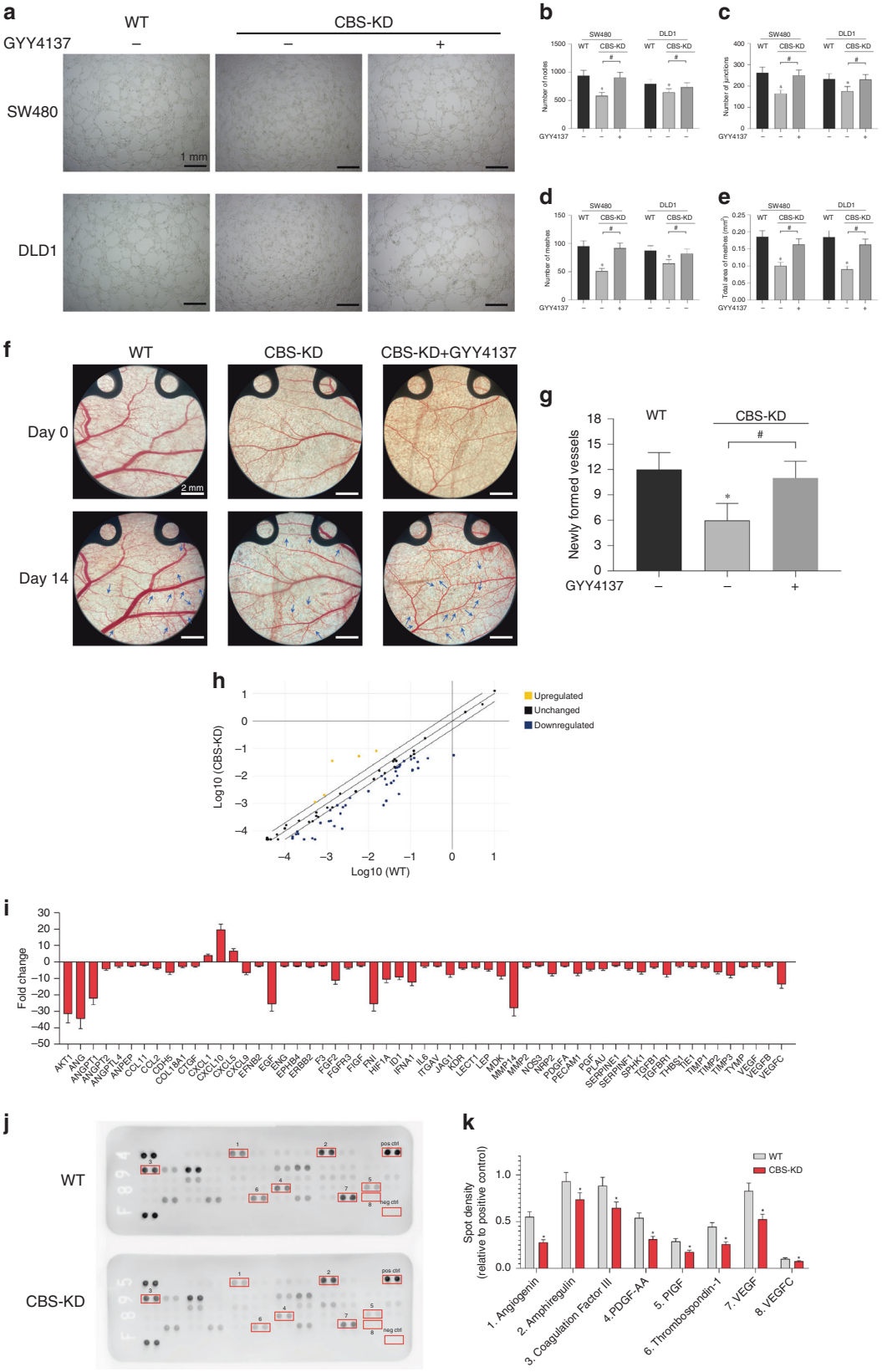

validated (Fig. 1g, h). The decreased release of H_2S in CBS-KD cells and cells incubated with sikokianin C was validated utilising lead acetate test papers (Fig. 1h). The CCK-8 assay indicated decreased proliferation of CBS-KD cells and cells incubated with sikokianin C compared with control cells (Fig. 1i, j). The scratch assay suggested that CBS-KD as well as sikokianin C inhibited the migration of

Fig. 2 Effect of CBS inhibition on angiogenesis of colon cancer cells. a Representative images of HUVECs after coculture with WT or CBS-KD SW480 and DLD1 cells with or without GYY4137 treatment. **b–e** Average numbers of nodes, junctions and meshes and the area ratio of meshes formed by HUVECs in different groups. **f** Representative images of capillary formation in the dorsal skinfold chamber in different groups. **g** Average number of newly formed vessels in different groups at 14 days. **h** Scatter plot of the RT2 Profiler PCR Array analysis results. **i** Fold changes in the transcript levels of genes associated with angiogenesis between WT and CBS-KD SW480 cells. (Genes with a transcription fold change >2 or < −2 are shown). **j** Representative images of the Proteome Profiler Human Angiogenesis Array. Spots with significant differences are marked with red boxes. Pos ctrl indicates the positive control, and neg ctrl indicates the negative control. **k** The densities of spots with significant differences. ($n = 3$, biological replicates) $^{*}P < 0.05$ vs. the control group. $^{\#}P < 0.05$ for the comparison between the two groups connected by brackets.

colon cancer cells (Fig. 1k, l, m). Transwell assays were further performed to investigate the effects of CBS-KD and Sikokianin C on cell migration and invasion, and the results were in accordance with those of the scratch assay, indicating decreased migration and invasion after CBS-KD or sikokianin C treatment in both cell lines (Fig. 1n–r).

Inhibiting CBS decreased the angiogenic effect of colon cancer cells both in vitro and in vivo

The angiogenic effect plays a vital role in the propagation and metastasis of colon cancer. Previous studies have focused on the physiological role of H_2S in promoting angiogenesis and dilating blood vessels. Our results in the coculture model of colon cancer cells and HUVECs indicated that CBS-KD inhibited the function of HUVECs, as evidenced by the decreased numbers of nodes and meshes formed by HUVECs cocultured with CBS-KD colon cancer cells. This inhibitory effect of CBS-KD was significantly alleviated by treatment with GYY4137 (50 μM), a slow-release donor of H_2S (Fig. 2a–e). The angiogenic effect of the CBS-H_2S axis in tumour cells was further investigated in vivo utilising the dorsal skinfold chamber model in mice. The results indicated that knocking out CBS in SW480 cells significantly inhibited tumour-associated angiogenesis and that this inhibition was attenuated by cotreatment with GYY4137 (Fig. 2f, g). Both PCR arrays and proteome arrays were adopted to investigate the mechanism underlying the angiogenic effect of the CBS-H_2S axis in colon cancer cells. The results indicated decreased mRNA expression of multiple angiogenesis-related genes after the knockout of CBS in SW480 cells (Fig. 2h, i). Proteome array analysis further validated the decreased levels of multiple angiogenic factors, including VEGF and VEGF-C, after knockout of CBS in SW480 cells (Fig. 2j, k). Based on these results, we investigated the correlation between VEGF and the CBS-H_2S axis and the underlying mechanisms.

Positive correlation between CBS and VEGF expression in colon cancer tissues

The expression of CBS was investigated by immunohistochemical analysis of a tissue microarray composed of 90 pairs of colon cancer tissues and adjacent normal tissues. The results indicated significantly increased expression of CBS in colon cancer tissues (Fig. 3a–c). In addition, a positive correlation was observed between CBS expression and tumour stage (Fig. 3d, e). Although there are data indicating that CBS expression is increased in colorectal adenocarcinoma tissues compared with normal tissues [29], increased CBS expression was associated with poorer survival in that cohort (Fig. 3f). The expression of VEGF was further investigated in the same tissue microarray, and the results indicated significantly increased expression of VEGF in colon cancer tissues (Fig. 3g, h). The staining intensity of both CBS and VEGF was evaluated with the histochemical scoring system, and a positive correlation was observed between CBS and VEGF in colon cancer tissues ($R^2 = 0.5946$, $P < 0.0001$) (Fig. 3i). No significant correlation between the expression of CBS and VEGF was observed in adjacent normal tissues, suggesting the tumour-specific effect of this positive correlation (Fig. 3j).

The positive feedback loop between VEGF and the CBS-H_2S axis

Significantly decreased expression of VEGF was evident after CBS-KD, and this decrease was lessened by cotreatment with GYY4137. GYY4137 also upregulated the expression of VEGF compared with that in control cells (Fig. 4a, c). Surprisingly, exogenous VEGF also upregulated the expression of CBS in SW480 cells, and this increase was lessened by cotreatment with bevacizumab, a commercial monoclonal antibody targeting VEGF. Bevacizumab also downregulated the expression of CBS compared with that in control cells (Fig. 4b, d). The changes in the mRNA levels of both CBS and VEGF were in accordance with the immunoblotting results, indicating the transcriptional origins of this reciprocal regulatory effect between VEGF and CBS (Fig. 4e, f). Analysis with the online tool Promoter Scan was performed on the promoter regions of both VEGF and CBS. We were very surprised to find that a potential AP-1 binding site was revealed in the promoter region of VEGF (Fig. 4g). Previous studies confirmed the regulatory effect of H_2S on the activity of AP-1 [30]. In addition, a potential NF-κB binding site was revealed in the promoter region of CBS (Fig. 4h). Intriguingly, the activation of NF-κB has been reported to be regulated by the VEGF signalling pathway [31]. The mRNA expression of AP-1 decreased after CBS knockdown (Fig. 4i), and the mRNA expression of NF-κB decreased after treatment with bevacizumab (Fig. 4j). Immunofluorescence staining and immunoblotting of both AP-1 and NF-κB indicated that the activation and nuclear translocation of AP-1 were regulated by the CBS-H_2S axis (Fig. 4k, l, o, q). However, the activation and nuclear translocation of NF-κB were regulated by VEGF signalling (Fig. 4m, n, p, r). Then, ChIP and dual-luciferase reporter assays were performed to confirm the regulatory effect of AP-1 on VEGF and NF-κB expression in cells with CBS knockdown. The results indicated that CBS-KD significantly decreased both the binding of AP-1 with the promoter region of VEGF and the transcriptional activity of the VEGF gene promoter; these decreases were lessened by GYY4137 treatment (Fig. 4s, u). Exogenous VEGF significantly increased both the binding of NF-κB with the promoter region of CBS and the transcriptional activity of the CBS gene promoter; these decreases were lessened by bevacizumab treatment (Fig. 4t, v). Together, these results validated a positive feedback loop between the CBS-H_2S axis and VEGF in colon cancer cells.

The synergistic effect of blocking CBS and VEGF in inhibiting liver metastasis of colon cancer cells

The positive correlation between CBS and VEGF expression led us to investigate the potential value of blocking both targets at the same time in colon cancer cells. A mouse model of liver metastasis was established by splenic injection of SW480 cells. The results indicated that treatment with bevacizumab or sikokianin C alone inhibited liver metastasis of colon cancer cells and that cotreatment with both reagents drastically decreased the number of metastatic nodules (Fig. 5a–c). Decreased metastasis of CBS-KD cells compared with WT cells was observed, and CBS-KD significantly increased the response to bevacizumab, as evidenced by the lowest liver weights and numbers of metastatic nodules in this group (Fig. 5c). Immunohistochemical

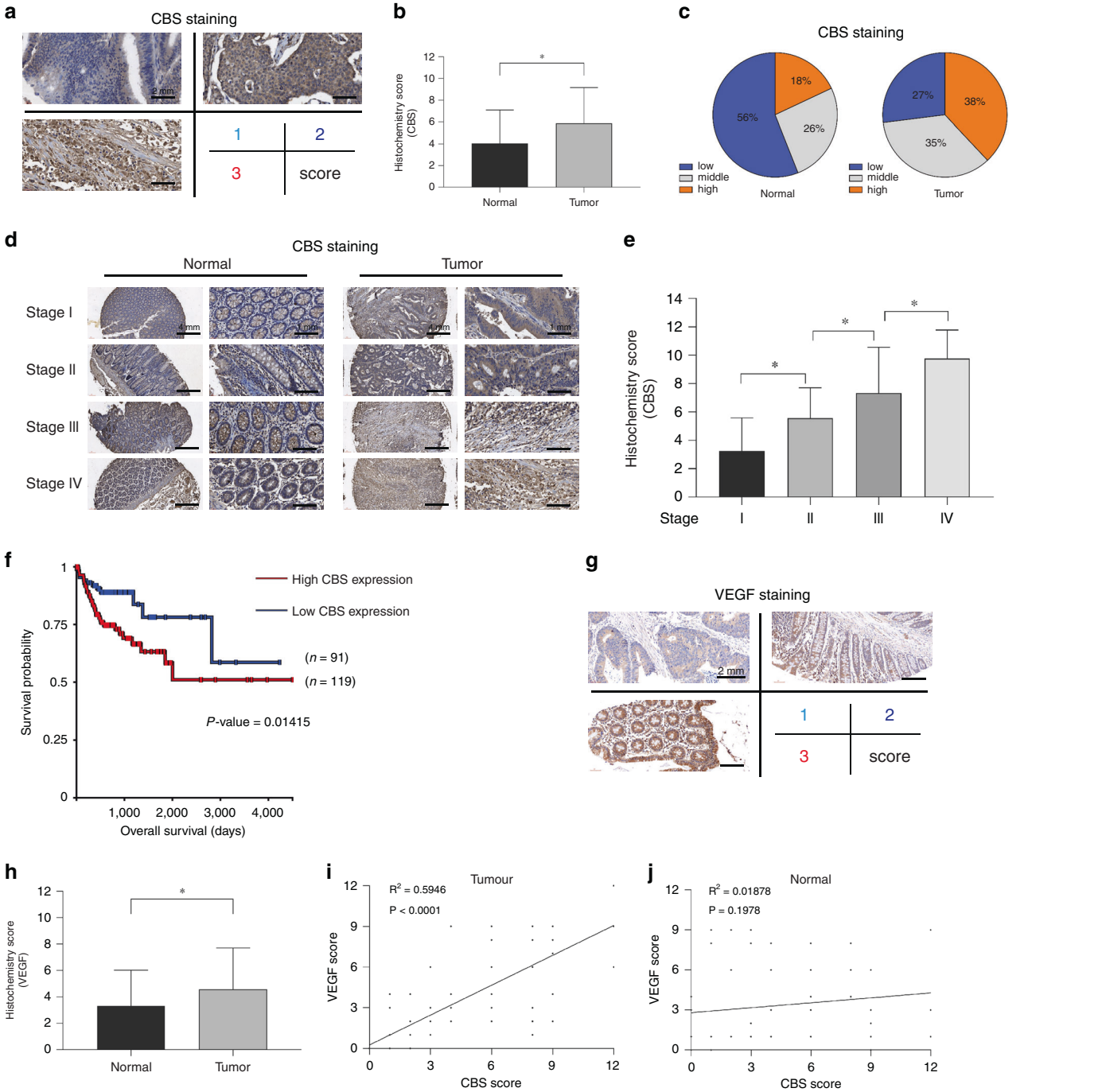

Fig. 3 The correlation between CBS and VEGF expression in colon cancer tissues. a Representative images of different levels of CBS immunohistochemical staining in the tissue microarray. **b** CBS histochemical score in the tumour tissues ($n = 90$) and adjacent normal tissues ($n = 90$) in the microarray. **c** The ratios of high, moderate and low expression regions in the tumour tissues and adjacent normal tissues in the microarray. **d** Representative images of CBS immunohistochemical staining in different-stage tumour tissues ($n = 90$) and adjacent normal tissues ($n = 90$) in the microarray. **e** Immunohistochemical score for CBS in different-stage colon tumour tissues in the microarray. (stage 1 = 28 cases; stage 2 = 28 cases; stage 3 = 21 cases; stage 4 = 13 cases). **f** Survival curve showing the impact of CBS expression on overall survival in the TCGA-OV dataset. (The figure was generated with UCSC Xena, https://xena.ucsc.edu/). **g** Representative images of different levels of VEGF immunohistochemical staining in the tissue microarray. **h** VEGF histochemical score in tumour tissues ($n = 90$) and adjacent normal tissues ($n = 90$) in the microarray. **i** Correlation analysis of the histochemical scores of CBS and VEGF in tumour tissues. **j** Correlation analysis of the histochemical scores of CBS and VEGF in adjacent normal tissues. *$P < 0.05$.

analysis was further performed to investigate the expression of VEGF and CD31 in metastatic lesions harvested from different groups (Fig. 5d–g). The results indicated that bevacizumab decreased both the VEGF and CD31 levels. Decreased VEGF and CD31 levels were evident in CBS-KD metastatic lesions, accompanied by loss of CBS expression. Sikokianin C, an inhibitor of CBS activity, decreased VEGF and CD31 levels and exerted no significant effect on the expression of CBS.

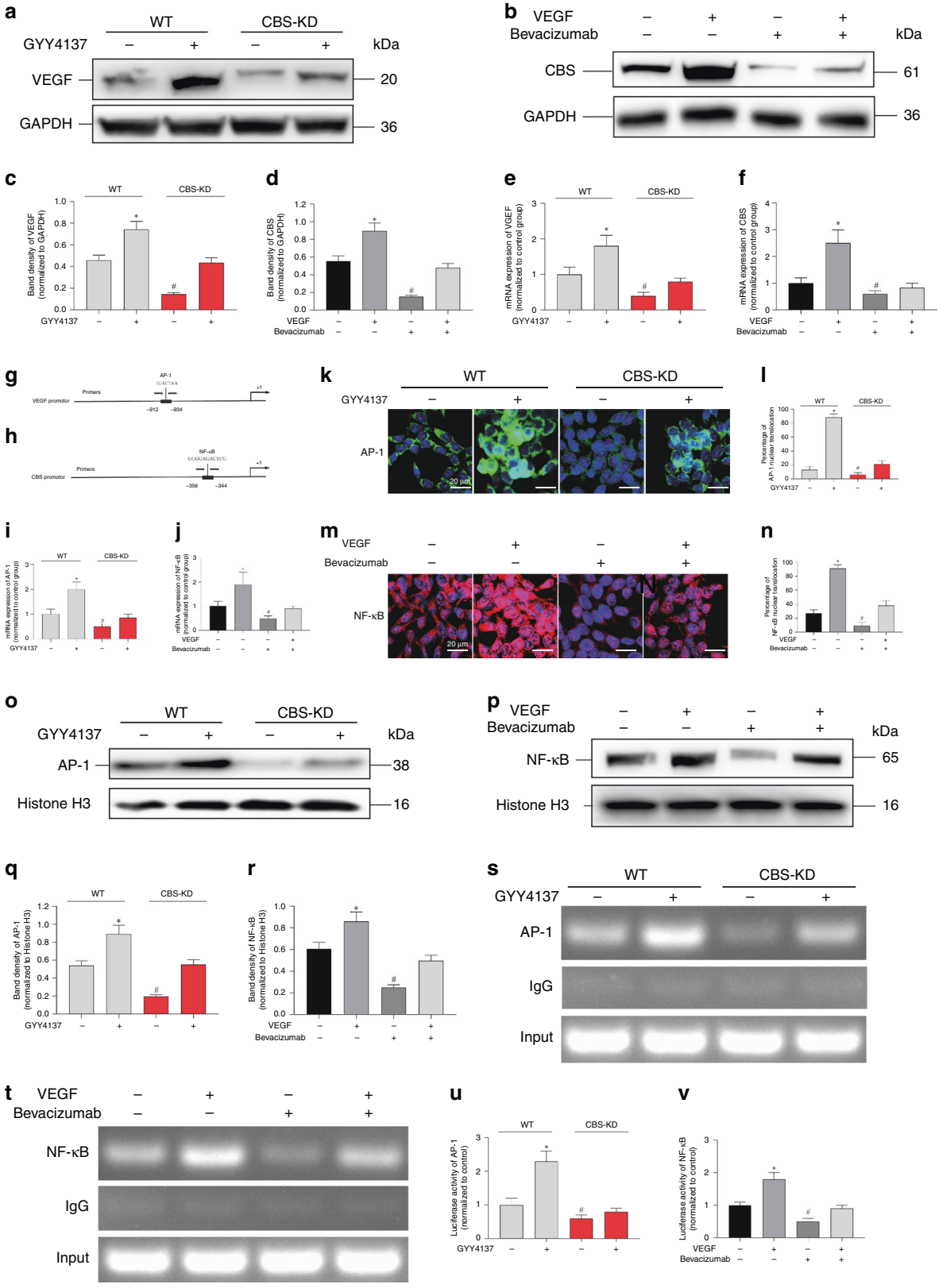

DISCUSSION

It is well known that the initiation, propagation and metastasis of tumour cells are closely related to their angiogenic capacity. Studies have shown that H_2S produced by tumours can be released through paracrine signalling into the tumour microenvironment and improve the tumour blood supply by promoting tumour-related angiogenesis and capillary dilation, thus facilitating tumour progression [32–34]. CBS is one of the major rate-limiting enzymes involved in endogenous H_2S production in tumour cells, producing H_2S during the conversion of homocysteine to cysteine [35]. Producers of H_2S,

Fig. 4 The effect of the CBS-H_2S axis on the activation of VEGF and the effect of VEGF on the activation of CBS. a, c Representative western blot images and relative band intensities of VEGF in SW480 WT and CBS-KD cells with or without GYY4137 treatment. GYY4137 (+) indicates that 50 μM GYY4137 was added, same as below. **b, d** Representative western blot images and relative band intensities of CBS in SW480 cells treated with VEGF with or without bevacizumab. VEGF (+) indicates that 30 ng/mL VEGF was added; bevacizumab (+) indicates that 3 μg/mL bevacizumab was added, as indicated below. **e** VEGF mRNA expression in SW480 WT and CBS-KD cells with or without GYY4137 treatment. **f** CBS mRNA expression in SW480 cells treated with VEGF with or without bevacizumab. **g, h** Schematic illustrations of the human VEGF gene promoter containing a putative AP-1 binding site and the human CBS gene promoter containing a putative NF-κB site. The PCR primer locations are also indicated. **i** AP-1 mRNA expression in SW480 WT and CBS-KD cells with or without GYY4137 treatment. **j** NF-κB mRNA expression in SW480 cells treated with VEGF with or without bevacizumab. **k**, **m** SW480 cells in different groups were subjected to immunofluorescence staining for AP-1 or NF-κB. **l** The percentage of AP-1 nuclear translocation. (N) The percentage of NF-κB nuclear translocation. **o**, **q** Representative western blot images and relative band intensities of AP-1 in the nucleus of SW480 WT and CBS-KD cells with or without GYY4137 treatment. **p**, **r** Representative western blot images and relative band intensities of NF-κB in the nucleus of SW480 cells treated with VEGF with or without bevacizumab. **s** ChIP analysis showed the binding of AP-1 to the promoter of VEGF in SW480 WT and CBS-KD cells with or without GYY4137 treatment. **t** ChIP analysis showed the binding of NF-κB to the promoter of CBS in SW480 cells treated with VEGF with or without bevacizumab. **u** Quantification of the fold change in VEGF promoter activity in SW480 WT and CBS-KD cells with or without GYY4137 treatment in luciferase reporter assays. A luciferase reporter plasmid containing the promoter region of VEGF was constructed (VEGF-luc). Cells were transfected with the VEGF-luc plasmid using Lipo3000 transfection reagent. **v** Quantification of the fold change in CBS promoter activity in SW480 cells treated with VEGF with or without bevacizumab in luciferase reporter assays. A luciferase reporter plasmid containing the promoter region of CBS was constructed (CBS-luc). Cells were transfected with the CBS-luc plasmid using Lipo3000 transfection reagent. ($n = 3$, biological replicates) * and # represent $P < 0.05$ vs. the control group.

including CBS, CSE and 3-MPST, have been shown to exhibit increased expression in multiple types of cancer tissues, such as colorectal, ovarian, kidney and breast cancers [36–38].

In this study, we used the colon cancer cell lines SW480 and DLD1 and generated the corresponding mutant cell lines with decreased expression of H_2S by knocking out the CBS gene. The scratch assay and Transwell assay results confirmed that CBS knockdown reduced invasion and metastasis. Coculture of colon cancer cells with HUVECs showed that CBS knockdown decreased the promotive effect of colon cancer cells on the tube formation ability of HUVECs. When colon cancer cells were implanted subcutaneously in vivo, CBS knockdown reduced the promotion of dorsal angiogenesis caused by colon cancer cells. PCR array analysis showed that CBS knockdown resulted in decreased levels of various angiogenesis-related mRNAs, and proteome array analysis showed decreased expression of various angiogenesis-related proteins, such as VEGF and VEGF-C. These results suggested that the effect of the CBS-H_2S axis on tumour angiogenesis is related to VEGF. By immunohistochemical staining and analysis of 90 pairs of tumour tissues and the corresponding adjacent normal tissues from colon cancer patients, we found a positive correlation between CBS and VEGF expression in tumour tissues. Furthermore, the western blot and RT–qPCR results showed that GYY4137 increased the transcription and expression of VEGF and that inhibition of CBS reduced the transcription and expression of VEGF. In addition, we were surprised to find that exogenous VEGF upregulated the transcription and expression of CBS and that bevacizumab, which is an anti-VEGF monoclonal antibody, inhibited the transcription and expression of CBS in colon cancer cells.

We analysed the promoter regions of both VEGF and CBS with the online tool Promoter Scan, and the results showed that there was a potential AP-1 binding site in the promoter region of VEGF and a potential NF-κB binding site in the promoter region of CBS. Previous studies have shown that H_2S can regulate the activity of AP-1, and coincidentally, the activation of NF-κB has been reported to be regulated by the VEGF signalling pathway [30, 31].

Therefore, we determined the expression levels of AP-1 and NF-κB in each group and investigated the binding sites of AP-1 in the promoter region of the CBS gene and NF-κB in the promoter region of the VEGF gene. IF, ChIP and dual-luciferase reporter assays were used to detect the binding of transcription factors to the corresponding gene promoter regions in each group. The results showed that CBS knockdown reduced the amount of AP-1 binding to the VEGF promoter region and the activation of the VEGF gene and that inhibition of VEGF by bevacizumab decreased the amount of NF-κB binding to the CBS promoter region and the activation of the CBS gene, which suggested a positive feedback loop between the CBS-H_2S axis and VEGF. Previous studies have shown that CBS inhibition suppresses patient-derived tumour xenograft (PDTX) growth in animal models and that PDTXs with increased CBS expression grow faster and respond better to CBS inhibitors [39, 40]. Finally, we established a mouse model of liver metastasis of colon cancer cells and found that CBS and VEGF blockers inhibited liver metastasis of colon cancer cells and that the combination of the two tested blockers (sikokianin C and bevacizumab) produced a synergistic effect.

Sikokianin C is a natural biflavonoid compound isolated from the medicinal herb *Stellera chamaejasme* that was identified as a selective inhibitor of recombinant CBS and showed no inhibition of CSE activity [41, 42]. In our study, sikokianin C inhibited tumour metastasis and angiogenesis, and these effects were closely related to its inhibition of CBS activity. However, the tumour inhibition mechanism of sikokianin C may not be limited to its inhibition of CBS activity. Studies have shown that biflavonoid compounds produce antitumour effects through a variety of molecular signalling pathways [43]. For example, delicaflavone can inhibit the PI3K/Akt/mTOR and Ras/MEK/Erk signalling pathways in rectal cancer cells through the mitochondrial ROS pathway [44], inhibit the MSPK signalling pathway in HeLa cervical cancer cells and induce apoptosis in G2/M phase [45]; hinokiflavone inhibits the induction of apoptosis via the NF-κB signalling pathway in liver cancer cells by activating the mitochondrial ROS/JNK/caspase pathway [46]. Whether sikokianin C exerts its antitumour effect through other pathways remains to be further studied.

In addition to focusing on the CBS-H_2S axis, a considerable number of recent studies have focused on the role of the 3-MPST-H_2S axis in tumours, which has received less attention in the past. Studies have shown that the expression of 3-MPST is upregulated in various cancer tissues and that this phenomenon is particularly prominent in cancer cells with multi-drug resistance phenotypes [29, 47, 48]. On the other hand, the use of 3-MPST inhibitors was found to inhibit the proliferation and migration of colon cancer cells [49, 50] and induce mesenchymal-epithelial transition in cancer cells [51]. These results, together with the results of our study, suggest that the synthase-H_2S axis plays an important role in tumour metabolism and that targeting H_2S synthases to inhibit tumour growth, metastasis and drug resistance is a promising direction.

In conclusion, we identified the role of the CBS-H_2S axis in angiogenesis and liver metastasis in colon cancer and found that the positive feedback between the CBS-H_2S axis and VEGF might be one of the underlying mechanisms. Furthermore, CBS may serve as a potential target in conversion therapy for liver metastasis of colon cancer.

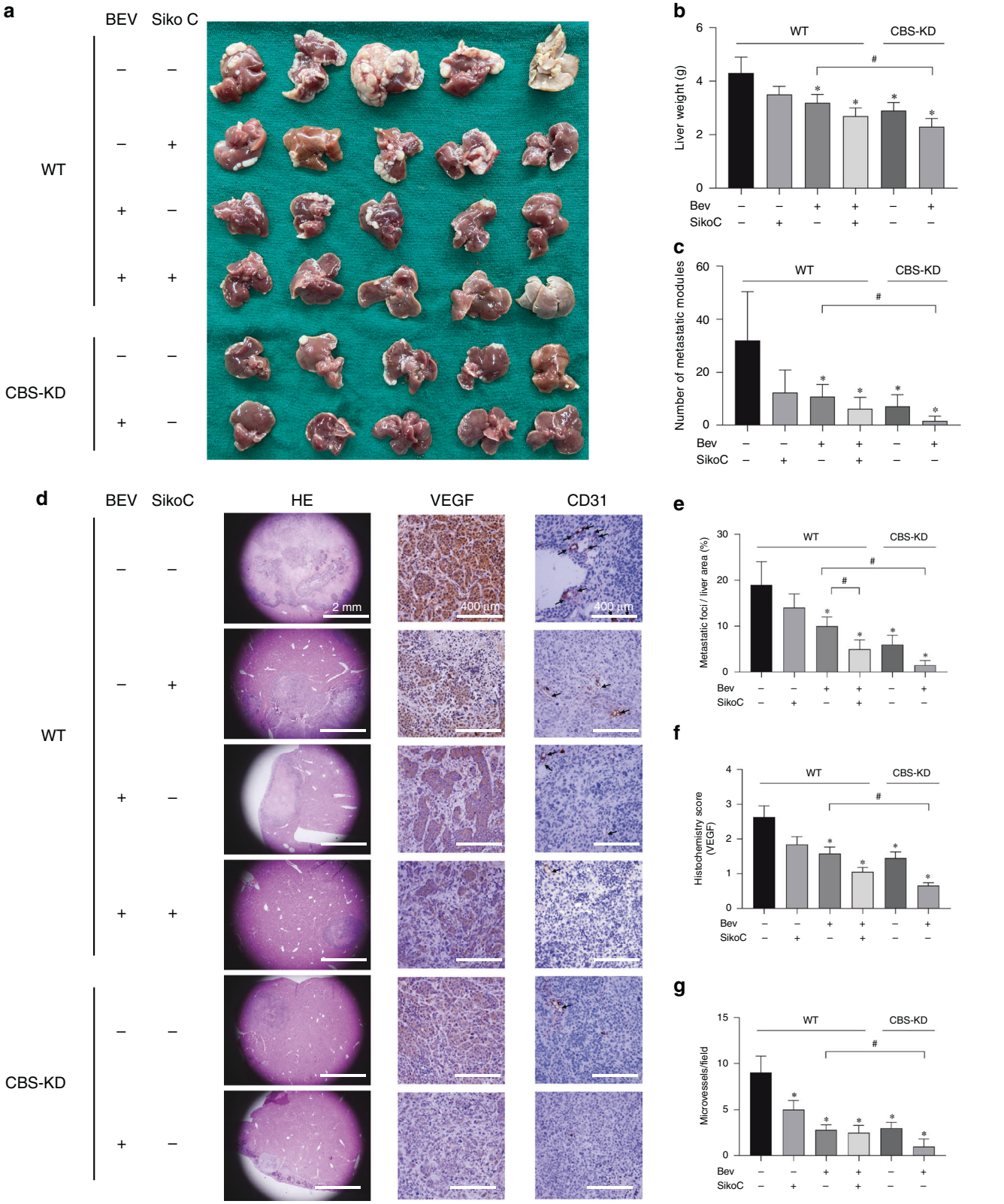

Fig. 5 The effect of CBS and VEGF on liver metastasis of colon cancer cells in vivo. a Images of liver metastatic nodules 6 weeks after tumour cell injection. Bev represents bevacizumab. **b** Average mouse liver weights in the 6 groups. ($n = 5$). **c** Average number of metastatic nodules. **d** Representative images of HE and immunohistochemical staining in liver tissue sections from the 6 groups. **e** Average area of metastatic foci in liver sections from the 6 groups. **f** VEGF histochemical score in liver tissue sections from the 6 groups. **g** Average number of microvessels stained with CD31 in liver tissue sections from the 6 groups. $^{*}P < 0.05$ vs. the control group. $^{\#}P < 0.05$ vs. the group of mice implanted with WT cells and treated with Bev (+) but not sikokianin C (−).

DATA AVAILABILITY

The data underlying this article are available in the article and in its online supplementary material.

REFERENCES

1. Sung H, Ferlay J, Siegel RL, Laversanne M, Soerjomataram I, Jemal A, et al. Global Cancer Statistics 2020: GLOBOCAN estimates of incidence and mortality worldwide for 36 cancers in 185 countries. CA Cancer J Clin. 2021;71:209–49.
2. Siriwardena AK, Mason JM, Mullamitha S, Hancock HC, Jegatheeswaran S. Management of colorectal cancer presenting with synchronous liver metastases. Nat Rev Clin Oncol. 2014;11:446–59.
3. Raoof M, Haye S, Ituarte PHG, Fong Y. Liver resection improves survival in colorectal cancer patients: causal-effects from population-level instrumental variable analysis. Ann Surg. 2019;270:692–700.
4. Dilek N, Papapetropoulos A, Toliver-Kinsky T, Szabo C. Hydrogen sulfide: an endogenous regulator of the immune system. Pharmacol Res. 2020;161:105119.
5. Li S, Liao R, Sheng X, Luo X, Zhang X, Wen X, et al. Hydrogen gas in cancer treatment. Front Oncol. 2019;6:9–696.
6. Chen L, Zhou SF, Su L, Song J. Gas-mediated cancer bioimaging and therapy. ACS Nano. 2019;13:10887–917.
7. Szabo C, Coletta C, Chao C, Módis K, Szczesny B, Papapetropoulos A, et al. Tumor-derived hydrogen sulfide, produced by cystathionine-β-synthase, stimulates bioenergetics, cell proliferation, and angiogenesis in colon cancer. Proc Natl Acad Sci USA. 2013;110:12474–9.
8. Wallace JL, Wang R. Hydrogen sulfide-based therapeutics: exploiting a unique but ubiquitous gasotransmitter. Nat Rev Drug Discov. 2015;14:329–45.
9. Vicente JB, Malagrinò F, Arese M, Forte E, Sarti P, Giuffrè A. Bioenergetic relevance of hydrogen sulfide and the interplay between gasotransmitters at human cystathionine β-synthase. Biochim Biophys Acta. 2016;1857:1127–38.
10. Wang YH, Huang JT, Chen WL, Wang RH, Kao MC, Pan YR, et al. Dysregulation of cystathionine γ-lyase promotes prostate cancer progression and metastasis. EMBO Rep. 2019;20:e45986.
11. Wang M, Yan J, Cao X, Hua P, Li Z. Hydrogen sulfide modulates epithelial-mesenchymal transition and angiogenesis in non-small cell lung cancer via NF-κB activation. Biochem Pharmacol. 2020;172:113775.
12. Untereiner AA, Pavlidou A, Druzhyna N, Papapetropoulos A, Hellmich MR, Szabo C. Drug resistance induces the upregulation of H2S-producing enzymes in HCT116 colon cancer cells. Biochem Pharmacol. 2018;149:174–85.
13. Chen S, Yue T, Huang Z, Zhu J, Bu D, Wang X, et al. Inhibition of hydrogen sulfide synthesis reverses acquired resistance to 5-FU through miR-215-5p-EREG/TYMS axis in colon cancer cells. Cancer Lett. 2019;466:49–60.
14. Chen S, Bu D, Zhu J, Yue T, Guo S, Wang X, et al. Endogenous hydrogen sulfide regulates xCT stability through persulfidation of OTUB1 at cysteine 91 in colon cancer cells. Neoplasia. 2021;23:461–72.
15. Pagano E, Elias JE, Schneditz G, Saveljeva S, Holland LM, Borrelli F, et al. Activation of the GPR35 pathway drives angiogenesis in the tumour microenvironment. Gut. 2021. https://gut.bmj.com/content/early/2021/04/08/gutjnl-2020-323363.long. Online ahead of print.
16. Cai WJ, Wang MJ, Moore PK, Jin HM, Yao T, Zhu YC. The novel proangiogenic effect of hydrogen sulfide is dependent on Akt phosphorylation. Cardiovasc Res. 2007;76:29–40.
17. Köhn C, Dubrovska G, Huang Y, Gollasch M. Hydrogen sulfide: potent regulator of vascular tone and stimulator of angiogenesis. Int J Biomed Sci. 2012;8:81–6.
18. Lei Y, Zhen Y, Zhang W, Sun X, Lin X, Feng J, et al. Exogenous hydrogen sulfide exerts proliferation, anti-apoptosis, angiopoiesis and migration effects via activating HSP90 pathway in EC109 cells. Oncol Rep. 2016;35:3714–20.
19. Chao C, Zatarain JR, Ding Y, Coletta C, Mrazek AA, Druzhyna N, et al. Cystathionine-beta-synthase inhibition for colon cancer: enhancement of the efficacy of aminooxyacetic acid via the prodrug approach. Mol Med. 2016;22:361–79.
20. Augsburger F, Randi EB, Jendly M, Ascencao K, Dilek N, Szabo C. Role of 3-mercaptopyruvate sulfurtransferase in the regulation of proliferation, migration, and bioenergetics in murine colon cancer cells. Biomolecules. 2020;10:447.
21. Bantzi M, Augsburger F, Loup J, Berset Y, Vasilakaki S, Myrianthopoulos V, et al. Novel aryl-substituted pyrimidones as inhibitors of 3-mercaptopyruvate sulfurtransferase with antiproliferative efficacy in colon cancer. J Med Chem. 2021;64:6221–40.
22. Ascenção K, Dilek N, Augsburger F, Panagaki T, Zuhra K, Szabo C. Pharmacological induction of mesenchymal-epithelial transition via inhibition of H2S biosynthesis and consequent suppression of ACLY activity in colon cancer cells. Pharmacol Res. 2021;165:105393.
23. Ye D, Guo S, Al-Sadi R, Ma TY. MicroRNA regulation of intestinal epithelial tight junction permeability. Gastroenterology. 2011;141:1323–33.
24. Zhang K, Zhang J, Xi Z, Li LY, Gu X, Zhang QZ, et al. A new H_2S-specific near-infrared fluorescence-enhanced probe that can visualize the H_2S level in colorectal cancer cells in mice. Chem Sci. 2017;8:2776–81.
25. Gaustad JV, Brurberg KG, Simonsen TG, Mollatt CS, Rofstad EK. Tumor vascularity assessed by magnetic resonance imaging and intravital microscopy imaging. Neoplasia. 2008;10:354–62.
26. Li X, Ma C, Zhang L, Li N, Zhang X, He J, et al. LncRNAAC132217.4, a KLF8-regulated long non-coding RNA, facilitates oral squamous cell carcinoma metastasis by upregulating IGF2 expression. Cancer Lett. 2017;407:45–56.
27. Guo S, Chen S, Ma J, Ma Y, Zhu J, Ma Y, et al. Escherichia coli nissle 1917 protects intestinal barrier function by inhibiting NF-κB-mediated activation of the MLCK-P-MLC signaling pathway. Mediators Inflamm. 2019. https://www.hindawi.com/journals/mi/2019/5796491/.
28. Chang Y, Liu C, Yang J, Liu G, Feng F, Tang J, et al. MiR-20a triggers metastasis of gallbladder carcinoma. J Hepatol. 2013;59:518–27.
29. Silver DJ, Roversi GA, Bithi N, Wang SZ, Troike KM, Neumann CK. Severe consequences of a high-lipid diet include hydrogen sulfide dysfunction and enhanced aggression in glioblastoma. J Clin Invest. 2021;131:e138276.
30. Xie L, Feng H, Li S, Meng G, Liu S, Tang X, et al. SIRT3 mediates the antioxidant effect of hydrogen sulfide in endothelial cells. Antioxid Redox Signal. 2016;24:329–43.
31. Chen C, You F, Wu F, Luo Y, Zheng G, Xu H, et al. Antiangiogenesis efficacy of ethanol extract from Amomum tsaoko in ovarian cancer through inducing ER stress to suppress p-STAT3/NF-κB/IL-6 and VEGF loop. Evid Based Complement Altern Med. 2020;2020:2390125.
32. Lopes-Coelho F, Martins F, Hipólito A, Mendes C, Sequeira CO, Pires RF, et al. The activation of endothelial cells relies on a ferroptosis-like mechanism: novel perspectives in management of angiogenesis and cancer therapy. Front Oncol. 2021;11:656229.
33. Wu D, Li J, Zhang Q, Tian W, Zhong P, Liu Z, et al. Exogenous hydrogen sulfide regulates the growth of human thyroid carcinoma cells. Oxid Med Cell Longev. 2019;2019:6927298.
34. Wu D, Li M, Tian W, Wang S, Cui L, Li H, et al. Hydrogen sulfide acts as a double-edged sword in human hepatocellular carcinoma cells through EGFR/ERK/MMP-2 and PTEN/AKT signaling pathways. Sci Rep. 2017;7:5134.
35. Szabo C. Gasotransmitters in cancer: from pathophysiology to experimental therapy. Nat Rev Drug Discov. 2016;15:185–203.
36. Chakraborty PK, Murphy B, Mustafi SB, Dey A, Xiong X, Rao G, et al. Cystathionine β-synthase regulates mitochondrial morphogenesis in ovarian cancer. FASEB J. 2018;32:4145–57.
37. Shackelford RE, Abdulsattar J, Wei EX, Cotelingam J, Coppola D, Herrera GA. Increased nicotinamide phosphoribosyltransferase and cystathionine-β-synthase in renal oncocytomas, renal urothelial carcinoma, and renal Clear cell carcinoma. Anticancer Res. 2017;37:3423–7.
38. Sen S, Kawahara B, Gupta D, Tsai R, Khachatryan M, Roy-Chowdhuri S, et al. Role of cystathionine β-synthase in human breast cancer. Free Radic Biol Med. 2015;86:228–38.
39. Hellmich MR, Coletta C, Chao C, Szabo C. The therapeutic potential of cystathionine β-synthetase/hydrogen sulfide inhibition in cancer. Antioxid Redox Signal. 2015;22:424–48.
40. Hellmich MR, Chao C, Módis K, Ding Y, Zatarain JR, Thanki K, et al. Efficacy of novel aminooxyacetic acid prodrugs in colon cancer models: towards clinical translation of the cystathionine β-synthase inhibition concept. Biomolecules. 2021;11:1073.
41. Niu W, Wu P, Chen F, Wang J, Shang X, Xu C. Discovery of selective cystathionine β-synthase inhibitors by high-throughput screening with a fluorescent thiol probe. Medchemcomm. 2016;8:198–201.
42. Niu W, Wu P, Chen F, Wang J, Shang X, Xu C. Discovery of selective cystathionine β-synthase inhibitors by high-throughput screening with a fluorescent thiol probe. Medchemcomm. 2016;8:198–201.
43. He X, Yang F, Huang X. Proceedings of chemistry, pharmacology, pharmacokinetics and synthesis of biflavonoids. Molecules. 2021;26:6088.
44. Yao W, Lin Z, Shi P, Chen B, Wang G, Huang J, et al. Delicaflavone induces ROS-mediated apoptosis and inhibits PI3K/AKT/mTOR and Ras/MEK/Erk signaling pathways in colorectal cancer cells. Biochem Pharmacol. 2020;171:113680.
45. Yao W, Lin Z, Wang G, Li S, Chen B, Sui Y, et al. Delicaflavone induces apoptosis via mitochondrial pathway accompanying G2/M cycle arrest and inhibition of MAPK signaling cascades in cervical cancer HeLa cells. Phytomedicine. 2019;62:152973.
46. Mu W, Cheng X, Zhang X, Liu Y, Lv Q, Liu G, et al. Hinokiflavone induces apoptosis via activating mitochondrial ROS/JNK/caspase pathway and inhibiting NF-κB activity in hepatocellular carcinoma. J Cell Mol Med. 2020;24:8151–65.
47. Zuhra K, Tomé CS, Masi L, Giardina G, Paulini G, Malagrinò F, et al. N-acetylcysteine serves as substrate of 3-mercaptopyruvate sulfurtransferase and stimulates sulfide metabolism in colon cancer cells. Cells. 2019;8:828.

48. Augsburger F, Szabo C. Potential role of the 3-mercaptopyruvate sulfurtransferase (3-MST)-hydrogen sulfide (H2S) pathway in cancer cells. Pharmacol Res. 2020;154:104083.
49. Bantzi M, Augsburger F, Loup J, Berset Y, Vasilakaki S, Myrianthopoulos V, et al. Novel aryl-substituted pyrimidones as inhibitors of 3-mercaptopyruvate sulfurtransferase with antiproliferative efficacy in colon cancer. J Med Chem. 2021;64:6221–40.
50. Augsburger F, Randi EB, Jendly M, Ascencao K, Dilek N, Szabo C. Role of 3-mercaptopyruvate sulfurtransferase in the regulation of proliferation, migration, and bioenergetics in murine colon cancer cells. Biomolecules. 2020;10:447.
51. Ascenção K, Dilek N, Augsburger F, Panagaki T, Zuhra K, Szabo C. Pharmacological induction of mesenchymal-epithelial transition via inhibition of H2S biosynthesis and consequent suppression of ACLY activity in colon cancer cells. Pharmacol Res. 2021;165:105393.

ACKNOWLEDGEMENTS

We would like to thank Professor Yi Long and Professor Ding-fang Bu for their excellent technical assistance.

AUTHOR CONTRIBUTIONS

SG: designed the study; performed experiments; wrote, reviewed and edited the manuscript. JL: performed experiments. ZH: performed experiments. TY: performed experiments. JL: performed experiments. JZ: provided resources. XW: provided resources. YL: designed the study. PW: designed the study; wrote, reviewed and edited the manuscript. SC: designed the study; performed experiments; wrote, reviewed and edited the manuscript.

FUNDING

This research was supported by the National Natural Science Foundation of China (No. 81902384).

COMPETING INTERESTS

The authors declare no competing interests.

ETHICS APPROVAL STATEMENT

The experimental protocol complied with the Guide for Care and Use of Laboratory Animals and was authorised by the Institutional Animal Care and Use Committee of Peking University for the use of experimental animals (No. J201965). All animal studies were complied with relevant ethical regulations for animal testing and research.

ADDITIONAL INFORMATION

Supplementary information The online version contains supplementary material available at https://doi.org/10.1038/s41416-021-01681-7.

Correspondence and requests for materials should be addressed to Shanwen Chen.

Reprints and permission information is available at http://www.nature.com/reprints

Publisher's note Springer Nature remains neutral with regard to jurisdictional claims in published maps and institutional affiliations.